frontiers | Frontiers in Physics

TYPE Original Research
PUBLISHED 04 April 2024
DOI 10.3389/fphy.2024.1378521

Check for updates

OPEN ACCESS

EDITED BY
Ciprian Catana,
Massachusetts General Hospital and Harvard Medical School, United States

REVIEWED BY
Charalampos Tsoumpas,
University Medical Center Groningen, Netherlands
Bo Zhou,
Yale University, United States

*CORRESPONDENCE
Daria Ferrara,
daria.ferrara@meduniwien.ac.at

RECEIVED 29 January 2024
ACCEPTED 18 March 2024
PUBLISHED 04 April 2024

CITATION
Ferrara D, Shiyam Sundar LK, Chalampalakis Z, Geist BK, Gompelmann D, Gutschmayer S, Hacker M, Kertész H, Kluge K, Idzko M, Langsteger W, Yu J, Rausch I and Beyer T (2024), Low-dose and standard-dose whole-body [18F]FDG-PET/CT imaging: implications for healthy controls and lung cancer patients. *Front. Phys.* 12:1378521.
doi: 10.3389/fphy.2024.1378521

COPYRIGHT
© 2024 Ferrara, Shiyam Sundar, Chalampalakis, Geist, Gompelmann, Gutschmayer, Hacker, Kertész, Kluge, Idzko, Langsteger, Yu, Rausch and Beyer. This is an open-access article distributed under the terms of the Creative Commons Attribution License (CC BY). The use, distribution or reproduction in other forums is permitted, provided the original author(s) and the copyright owner(s) are credited and that the original publication in this journal is cited, in accordance with accepted academic practice. No use, distribution or reproduction is permitted which does not comply with these terms.

Low-dose and standard-dose whole-body [18F]FDG-PET/CT imaging: implications for healthy controls and lung cancer patients

Daria Ferrara[1]*, Lalith Kumar Shiyam Sundar[1], Zacharias Chalampalakis[1], Barbara Katharina Geist[2], Daniela Gompelmann[3], Sebastian Gutschmayer[1], Marcus Hacker[2], Hunor Kertész[4], Kilian Kluge[2], Marco Idzko[3], Werner Langsteger[2], Josef Yu[2], Ivo Rausch[1] and Thomas Beyer[1]

[1]QIMP Team, Medical University of Vienna, Vienna, Austria, [2]Department of Biomedical Imaging and Image-Guided Therapy, Division of Nuclear Medicine, Medical University of Vienna, Vienna, Austria, [3]Division of Pulmonology, Department of Internal Medicine II, Medical University Vienna, Vienna, Austria, [4]Image X Institute, Faculty of Medicine and Health, The University of Sidney, Sidney, NSW, Australia

Aim: High-sensitivity hybrid positron emission tomography (PET) imaging using advanced whole-body (WB) or total-body PET/computed tomography (CT) systems permits reducing injected tracer activity while preserving diagnostic quality. Such approaches are promising for healthy control studies or exploring inter-organ communication in systemic diseases. This study assessed test/retest variations in the fluoro-2-deoxy-D-glucose (FDG) uptake in key organs from low-dose (LD) and standard-dose (STD) [18F]FDG-PET/CT imaging protocols in healthy controls and lung cancer patients.

Methods: A total of 19 healthy controls (19–62 years, 46–104 kg, 10 M/9 F) and 7 lung cancer patients (47–77 years, 50–88 kg, 4 M/3 F) underwent [18F]FDG-PET/CT imaging. All subjects were first injected ("test," LD) with 28 ± 2 MBq FDG and underwent a dynamic (0–67 min post-injection) WB imaging protocol with LD-CT. Then, 90 min post-LD injection, the subjects were repositioned and injected with 275 ± 16 MBq FDG ("retest," STD). Second LD-CT and STD-CT scans were acquired for healthy controls and patients, respectively. Static images (55–67 min post-injection) were considered for subsequent analysis. The CT images were used to automatically segment the target volumes of interest. Standardized uptake values normalized to the body weight (SUV_{BW}) were extracted for each volume of interest. The mean SUV_{BW} were compared for both LD/STD conditions with paired t-tests. In patients, FDG-avid lesions were manually delineated on LD and STD static images. Effective dose levels were estimated from both the CT and PET acquisitions.

Results: Organ-based mean SUV_{BW} were similar between the LD and STD (mean %difference ≤5%) in both healthy controls and cancer patients, except in the heart. Intra-control test/retest variability was significant in the brain, heart, and skeletal muscle ($p < 0.05$). While 17 lesions were delineated on the STD images of the patients, only 10/17 lesions were identified on the LD images due to increased image noise. Lesion-based mean SUV_{BW} were similar between LD and STD

acquisitions (p = 0.49, %difference = 10%). In patients, the effective doses were (1.9 ± 0.2) mSv (LD-CT), (16.6 ± 5.4) mSv (STD-CT), (0.5 ± 0.1) mSv (LD-PET), and (4.6 ± 0.3) mSv (STD-PET).

Conclusion: LD and STD [18F]FDG injections in healthy controls and lung cancer patients yielded comparable mean SUV_{BW}, except in the heart. Dose levels may be reduced for [18F]FDG-PET imaging without a loss in mean SUV_{BW} accuracy, promoting LD-PET/CT protocols for studying multi-organ metabolic patterns. In oncology patients, this approach may be hindered by a lower diagnostic quality in the presence of significant noise.

KEYWORDS

PET/CT, low-activity imaging, radiation exposure, [18F]fluoro-2-deoxy-D-glucose, standardized uptake values

Introduction

Since its inception in the late 1990s [1], hybrid positron emission tomography (PET) and computed tomography (CT), also referred to as dual-modality PET/CT, has become a well-established non-invasive imaging modality for a wide variety of clinical applications. In many oncology indications, PET/CT has been accepted as a standard imaging modality in patient management, providing both metabolic and anatomic information for diagnosis and treatment planning [2–4].

The technological innovations of recent years, culminating in the introduction of total-body (TB) PET/CT systems [5], have brought continuous improvements in system performance and sensitivity [6, 7] and consequently expanded PET/CT imaging to new research areas. For instance, the advent of extended axial field-of-view PET systems allows the simultaneous and quantitative imaging of multiple distant organs, thereby providing the possibility to investigate multi-organ metabolic information and detect potential anomalies from normal metabolic activity patterns [8, 9]. To visualize and quantify metabolic aberrations, it is necessary to establish a normative, organ- or voxel-wise, database based on the images derived from healthy controls. However, to create such a database, a significant amount of data must be collected first in light of the public concerns over ionizing radiation. Radiation exposure from PET/CT imaging, as measured by the effective dose to a subject, scales with the amount of injected PET tracer activity. The new PET/CT systems, with their increased sensitivity, allow for further reduction in injected tracer activity and, subsequently, reduction in radiation exposure [7, 10, 11].

Prior studies of low-dose PET/CT imaging have indicated potential for their adoption in clinical routine. For example, Calderón et al. demonstrated that decreasing levels of injected [18F]fluoro-2-deoxy-D-glucose (FDG) activity ranging from 3.0 MBq/kg to 0.125 MBq/kg affected the mean standardized uptake values (SUVs) by only 8% or less [11]. Kertész et al. investigated the effects of reducing the injected [18F]FDG activity in pediatric oncology patients undergoing whole-body PET/CT examinations and showed that the injected activity levels can be reduced to 75% of the original dose without compromising the PET image quality [12]. Prieto et al. evaluated the impact of a 30% FDG dose reduction on image quality, resulting in steady clinical reading confidence despite a slight reduction in image quality [13]. Taken together, these studies either focused solely on deriving low-count PET images from standard activity images via list-mode resampling rather than using actual low-activity injections or they relied on the improved sensitivity of TB-PET systems, which are not yet widely available in medical facilities. Adding to the above research, Tan et al. compared ultra-low-dose and half-dose [18F]FDG-TB-PET/CT imaging in a test–retest setup within a 72-h time frame [14]. However, this study focused primarily on parametric imaging and assessed SUVs exclusively in the liver, thereby neglecting other organs and the continuous predominance of semi-quantitative SUV evaluations over kinetic modeling in clinical routine [15].

Our study, preceding the installation of a TB-PET/CT system, assesses the impact of reduced PET tracer doses on quantitative organ-based SUV_{BW} measurements, especially in healthy controls. Focusing on [18F]FDG imaging, we seek to understand the effects of lowering injected tracer doses on healthy organ evaluations and

TABLE 1 Demographics of study participants.

Healthy controls	
n° participants	19
Median age (years, range)	32 (19–62)
Average age (years, mean ± SD)	35 ± 14
Height (cm, mean ± SD)	175 ± 12
Weight (kg, mean ± SD)	76 ± 17
BMI (kg/m^2, mean ± SD)	25 ± 5
Injected low dose (MBq, mean ± SD, "test")	28 ± 2
Injected standard dose (MBq, mean ± SD, "retest")	279 ± 14
Lung cancer patients	
n° participants	7
Median age (years, range)	65 (47–77)
Average age (years, mean ± SD)	62 ± 13
Height (cm, mean ± SD)	165 ± 11
Weight (kg, mean ± SD)	71 ± 14
BMI (kg/m^2, mean ± SD)	26 ± 4
Injected low dose (MBq, mean ± SD, "test")	29 ± 3
Injected standard dose (MBq, mean ± SD, "retest")	271 ± 17

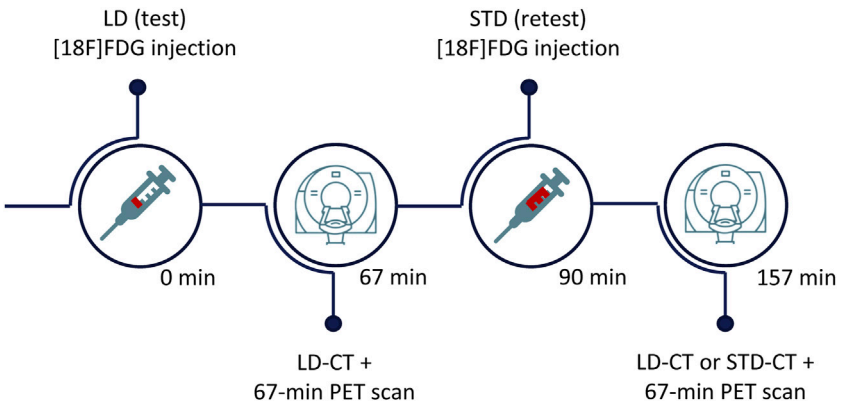

FIGURE 1
Visual description of the study protocol.

disease-related metabolic changes. Using serial [18F]FDG injections (test/retest), we examined intra-subject variabilities over 90 min and compared lesion uptake variations between low-dose (LD) and standard-dose (STD) PET scans in lung cancer patients. The goal was to create a standard organ-SUV_{BW} database for analyzing metabolic discrepancies due to diseases [9] and reduce radiation concerns from PET/CT scans.

Materials and methods

Participants

The study included 19 healthy controls (19–62 years, 46–104 kg, 10 M/9 F) and 7 lung cancer patients (47–77 years, 50–88 kg, 4 M/3 F). Here, "healthy" means the clinical absence of known systemic diseases. All data were acquired according to the Declaration of Helsinki (EK1907/2020) between July and December 2021. Written informed consent was obtained from all the subjects before examinations. The details of the participants' demographics are summarized in Table 1. Statistics are reported as the mean ± standard deviation (SD).

Imaging protocol

All participants were scanned on a Siemens Biograph Vision 600 PET/CT system with an axial field-of-view of 26.3 cm and time-of-flight (TOF) resolution of 220 ps [16]. The participants were asked to fast for 6 h before the examinations and were scanned in supine position with their arms down. Each subject first underwent a 67-min PET acquisition following an LD intravenous injection of [18F]FDG (28 ± 2 MBq, 10% of the National Diagnostic Reference Levels of Austria [17]). After completing the acquisition, the subjects were given a 20-min break to empty their bladder.

Then, 90 min post-LD injection, the subjects were repositioned and injected with a bolus of [18F]FDG (275 ± 16 MBq), followed by a 67-min acquisition (STD) (Figure 1). The first 6 min of both PET protocols were performed with the patient fixed to the table to cover the chest region, followed by 14 whole-body (WB) sweeps under continuous table motion, adding up to a total emission scan time of 61 min.

A CT scan (120 kVp, 35 mAs ref, CareDose tube current modulation enabled) was performed for the CT-based attenuation correction prior to each PET scan. Healthy controls were scanned using LD-CT (average dose length product, DLP = 133 ± 19 mGy*cm) for both the test (LD-PET) and retest (STD-PET). Lung cancer patients underwent an LD-CT (DLP = 121 ± 8 mGy*cm) for the test (LD-PET) and then STD-CT for standard clinical care (DLP = 1,144 ± 377 mGy*cm) in the retest scan (STD-PET). In the STD-CT protocol, dual-phase (venous and arterial phases) contrast-enhanced CT, including the entire body in the field-of-view, was used for both clinical reporting and attenuation correction.

PET images were reconstructed with a matrix size of 220 × 220 × 803 and a voxel size of 3.3 × 3.3 × 2 mm^3, using 3D PSF + TOF OSEM (4 iterations and 5 subsets) with all corrections applied and a 3-mm full-width at half-maximum (FWHM) Gaussian post-reconstruction filter.

Quantification of organs

In all acquisitions, LD-CT was used to automatically delineate different target volumes using the AI-based segmentation tool MOOSE [18]. The resulting segmentations included abdominal organs, bones, muscles, fat, and heart subregions. A complete list of the segmented regions is given in Supplementary Table S1 of Supplementary Materials. From the last 12 min of the static acquisitions (55–67 min post-injection) of both tracer activities, the mean SUVs normalized to the body weight (SUV_{BW}) were extracted for every volume of interest (VOI) and every participant. The mean SUV_{BW} extracted from the STD acquisitions were corrected according to Eq. 1, including the residual activity 90 min post-LD injection:

$$\text{Mean } SUV_{BW} = \frac{C_{VOI}\left[\frac{kBq}{mL}\right]}{A_{inj}[MBq] + A_{res}[MBq]} * BW[kg], \qquad (1)$$

where C_{VOI} is the activity concentration in the VOI, A_{inj} is the total injected activity, A_{res} is the residual activity 90 min post-LD

injection, and *BW* is the body weight [19]. The average SUV_{BW} and the corresponding standard deviations were evaluated for each VOI in both healthy controls and patients. Group averaged parameters were compared for both LD and STD conditions with %differences and unpaired sample t-tests. A p-value <0.05 was considered statistically significant. Intra-subject variability between the test–retest protocols was assessed with %differences and paired sample t-tests.

Lung cancer patients

The 3D Slicer [20] software was used to visualize the PET images of lung cancer patients. Otsu's method [21] was applied for image thresholding using the automatic option in 3D Slicer, highlighting regions in the images with pathologically increased signals (lesion). An experienced clinician manually fine-tuned lesion segmentations to visually refine lesion boundaries where necessary. FDG-avid lesions were first identified on LD-PET images and then on STD-PET images in order to prevent any potential bias caused by the improved image quality of the STD-PET data. The number of segmented lesions was compared to the clinical report of each patient.

The mean SUVs normalized for body weight were calculated for each lesion using data from the last 12 min of the PET acquisitions for both LD and STD. Corresponding volumes were extracted for both LD and STD acquisitions. The results were then compared using %differences and paired sample t-tests.

Literature comparison

The mean SUV_{BW} of organs in healthy controls undergoing STD-PET were compared to the SUV_{BW} ranges provided in [22], [23] (kidneys and skeletal muscle) and [24] (subcutaneous fat). References were chosen by ensuring that the study protocol (60 ± 10-min PET acquisitions with [18F]FDG) and participant demographics (age, sex, and weight distributions) were similar to those in the current study.

Effective dose estimations

Effective doses (EDs) were evaluated for both LD and STD protocols in healthy controls and lung cancer patients. Specifically, the radiation dose from the CT scans was estimated using the DLP multiplied by the conversion factor k, where k = 0.015 mSv/mGy*cm for whole-body CT examinations [25, 26]. The PET contribution to the effective dose was calculated by multiplying the injected activity with the dose coefficient Γ = 0.017 mSv/MBq for [18F]FDG [27]. The total effective doses were obtained by summing the individual CT and PET contributions, according to Eq. 2:

$$ED_{tot} = ED_{CT} + ED_{PET} = DLP[mGy^{*}cm]^{*}k\left[\frac{mSv}{mGy^{*}cm}\right] + A[MBq]^{*}\Gamma\left[\frac{mSv}{MBq}\right]. \quad (2)$$

The resulting effective doses for both LD and STD acquisitions were compared to dose estimates from the existing literature [28–31].

Results

Quantification of organs

Healthy controls

A complete list of the segmented regions, as well as the corresponding uptake values, is given in Supplementary Table S1 of Supplementary Materials. The mean SUV_{BW} of the target volumes ranged from 0.4 ± 0.1 (subcutaneous fat) to 6.4 ± 1.1 (brain) across healthy controls (Table 2). The mean SUV_{BW} from both LD and STD protocols were similar (absolute %difference ≤5%, Figure 2), except for the heart (absolute %difference = 14%). The group unpaired t-test underlined no statistical differences in any VOI ($p > 0.05$). In healthy controls, intra-subject variations in SUV_{BW} between test/retest scans were significant in the brain (average %difference = 5%, $p = 0.01$), heart (19%, $p = 0.04$), skeletal muscle (8%, $p = 0.01$), and adrenal glands (15%, $p = 0.03$) (Figure 3; Table 3).

Lung cancer patients

In lung cancer patients, the mean SUV_{BW} in the segmented regions varied, on average, from 0.4 ± 0.1 (subcutaneous fat) to 5.4 ± 1.0 (brain) (Table 4). In all the VOIs, the mean SUV_{BW} between test and retest scans were comparable (average absolute % difference ≤5%; Figure 4), except in the heart (20%). The group unpaired t-test indicated no statistical differences in any VOI ($p > 0.05$). Intra-patient changes in organ-based uptake values between test and retest scans were not significant (Figure 5; Table 5).

Lesion evaluation

A total of 10 FDG-avid lesions were observed and delineated on the LD images of the lung cancer patients. In contrast, 17 lesions were delineated on the STD images, a total number equivalent to the information provided in the clinical reports of the patients. Lesion volumes derived from LD images of the tumor were 41% smaller than those derived from the STD images (Supplementary Table S2). Seven lesions (<2 cm^3) were not detected on the LD-PET images (Figure 6). The mean SUV_{BW} values of correspondent lesions were similar in LD and STD acquisitions (10%, $p = 0.49$; Table 6). In patient #005, the lesion was visible only on the CT, and, therefore, no SUV was obtained.

Literature comparison

Organ-based mean SUV_{BW} values in the STD acquisitions of healthy controls were comparable to literature references (Figure 7). Across all organs, the assessed mean SUV_{BW} consistently fell within the ranges reported in previous studies [22–24]. Subcutaneous fat exhibited the least uptake values (0.4 ± 0.1), while the brain demonstrated the highest uptake (6.4 ± 1.1).

Effective dose estimations

For healthy controls, the average total effective dose was 2.5 ± 0.3 mSv for the test (LD-CT + LD-PET) and 6.7 ± 0.4 mSv for the

TABLE 2 Mean standardized uptake values normalized to the body weight (SUV_{BW}) group statistics for healthy controls.

Volume of interest	Test LD SUV_{BW}	Retest STD SUV_{BW}	Absolute difference (%)	Unpaired t-test
Brain	6.4 ± 1.1	6.6 ± 1.1	3	$p = 0.56$
Heart	3.0 ± 1.8	2.6 ± 1.5	14	$p = 0.46$
Kidneys	2.7 ± 0.5	2.8 ± 0.4	4	$p = 0.47$
Liver	2.0 ± 0.3	2.0 ± 0.3	1	$p = 0.85$
Pancreas	1.5 ± 0.2	1.5 ± 0.2	1	$p = 0.83$
Spleen	1.5 ± 0.2	1.5 ± 0.2	1	$p = 0.87$
Lung	0.6 ± 0.2	0.6 ± 0.1	5	$p = 0.49$
Skeletal muscle	0.6 ± 0.1	0.6 ± 0.1	5	$p = 0.25$
Subcutaneous fat	0.4 ± 0.1	0.4 ± 0.1	3	$p = 0.61$

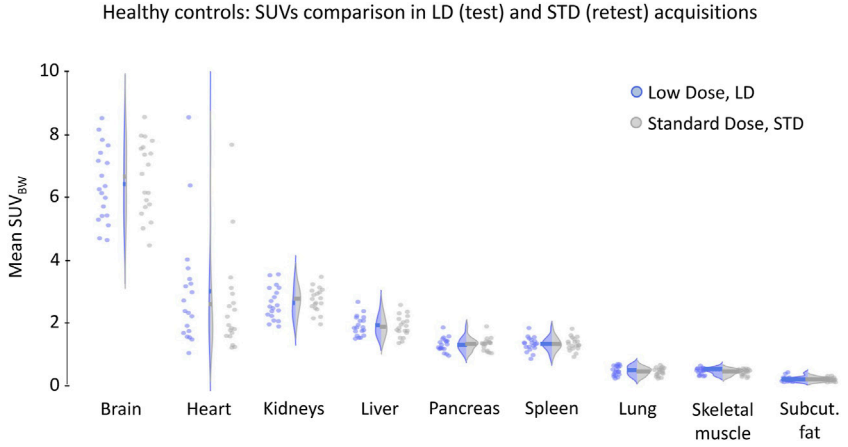

FIGURE 2
Comparison of the mean standardized uptake values normalized to the body weight (SUV_{BW}) in low-dose (LD) (blue, test) and standard-dose (STD) (gray, retest) acquisitions across 19 healthy controls.

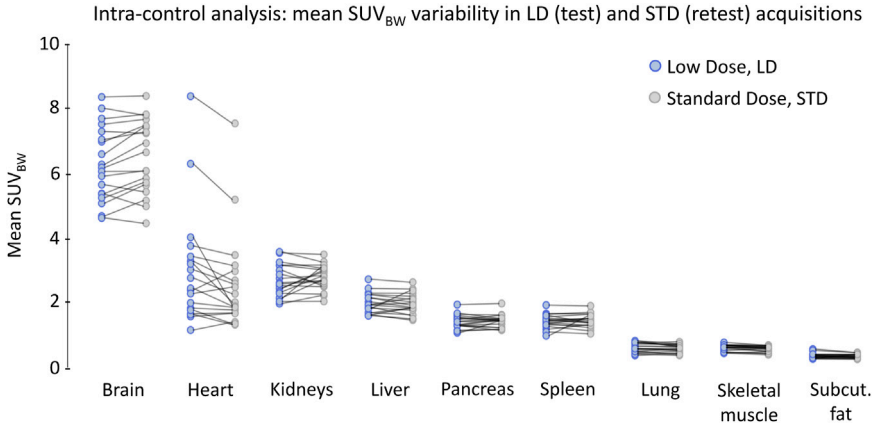

FIGURE 3
Intra-subject variability of the mean SUV_{BW} in LD (blue, test) and STD (gray, retest) acquisitions of 19 healthy controls.

TABLE 3 Intra-subject variability of the mean SUV_{BW} between LD/STD scans of healthy controls. Organs with statistically significant differences in LD/STD SUV are indicated in red.

Volume of interest	Absolute difference (%)	Paired t-test
Brain	5	$p = 0.01$
Heart	19	$p = 0.04$
Kidneys	10	$p = 0.21$
Liver	7	$p = 0.68$
Pancreas	7	$p = 0.63$
Spleen	8	$p = 0.77$
Lung	9	$p = 0.05$
Skeletal muscle	8	$p = 0.01$
Subcutaneous fat	8	$p = 0.24$

TABLE 4 Mean SUV_{BW} group statistics for lung cancer patients.

Volume of interest	Test LD SUV_{BW}	Retest STD SUV_{BW}	Absolute difference (%)	Unpaired t-test
Brain	5.3 ± 1.0	5.4 ± 0.9	2	$p = 0.79$
Heart	3.0 ± 1.8	3.0 ± 1.3	1	$p = 0.97$
Kidneys	2.9 ± 0.5	2.9 ± 0.3	1	$p = 0.85$
Liver	2.2 ± 0.4	2.3 ± 0.4	1	$p = 0.91$
Pancreas	1.5 ± 0.3	1.4 ± 0.2	3	$p = 0.74$
Spleen	1.6 ± 0.2	1.6 ± 0.1	2	$p = 0.74$
Lung	0.6 ± 0.2	0.6 ± 0.2	2	$p = 0.91$
Skeletal muscle	0.7 ± 0.1	0.6 ± 0.1	4	$p = 0.91$
Subcutaneous fat	0.4 ± 0.1	0.4 ± 0.1	3	$p = 0.91$

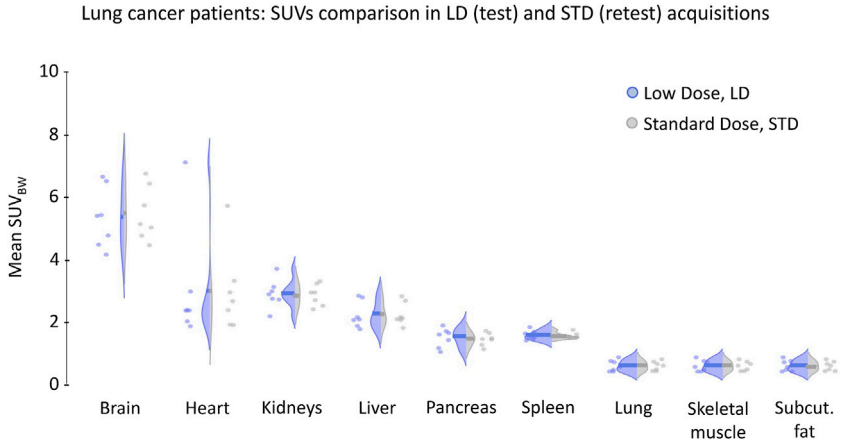

FIGURE 4
Comparison of the mean SUV_{BW} in LD (blue, test) and STD (gray, retest) acquisitions of seven lung cancer patients.

retest (LD-CT + STD-PET), respectively. The contribution from the PET scan to these total effective doses was 0.5 ± 0.1 mSv for the test (20%) and 4.8 ± 0.3 mSv for the retest acquisition (72%).

In cancer patients, the average effective dose contribution from the STD-CT was 16.6 ± 5.4 mSv (81%) to a total effective dose of 21.3 ± 5.4 mSv. With the LD-PET/CT protocol, the total effective

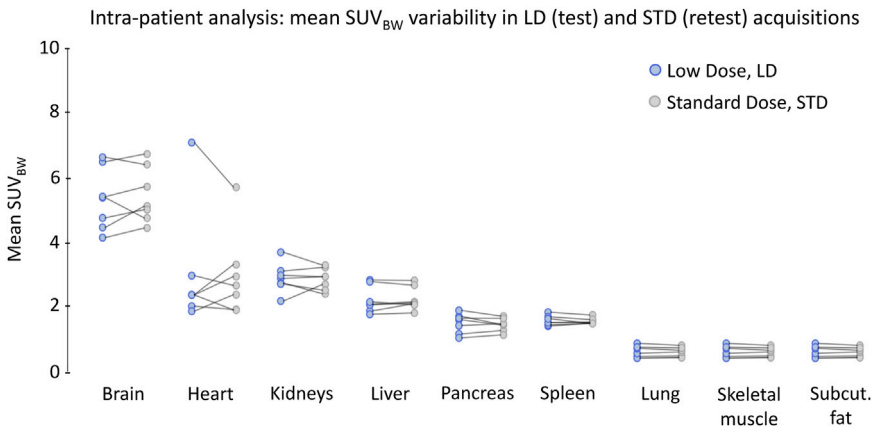

FIGURE 5
Intra-subject variability of the mean SUV_{BW} in LD (blue, test) and STD (gray, retest) acquisitions of seven lung cancer patients.

TABLE 5 Intra-subject variability of the mean SUV_{BW} between LD/STD scans of lung cancer patients.

Volume of interest	Absolute difference (%)	Paired t-test
Brain	7	$p = 0.44$
Heart	20	$p = 0.91$
Kidneys	8	$p = 0.74$
Liver	4	$p = 0.57$
Pancreas	8	$p = 0.42$
Spleen	4	$p = 0.47$
Lung	5	$p = 0.53$
Skeletal muscle	7	$p = 0.22$
Subcutaneous fat	4	$p = 0.16$

dose was reduced to 2.4 ± 0.1 mSv, while the relative contribution (1.9 ± 0.2 mSv) from the CT remained the same (79%). Table 7 summarizes the complete dose records in both groups of subjects.

Discussion

This study evaluated variations in organ uptake in [18F]FDG-PET/CT images of healthy controls and lung cancer patients undergoing a dual-injection, dual-scan protocol. We demonstrate similar uptake values in key organs for both LD- and STD-PET imaging, with an exception in the heart on a group-based level. Intra-subject variabilities were highest in the brain (7%), skeletal muscles (8%), and heart (20%). All mean SUV_{BW} were comparable with previously recorded literature values (Figure 7) [22–24]. While our study suggests equivalence of LD- and STD-PET imaging protocols for organ-based quantification in healthy controls, care must be taken when assessing patients since the LD protocol yielded a lower detection rate of actual lesions (Figure 6).

In the present study, test and retest [18F]FDG PET/CT scans were set apart by 90 min (Figure 1), without significant differences in the group mean SUV_{BW} in key organs (Figures 2, 4) in both healthy controls and lung cancer patients. The intra-subject variability in organ uptakes between LD and STD was also explored. Significant changes in the mean uptake values from test to retest scans of healthy controls were observed in the brain, heart, adrenal glands, and, to a lesser extent, in skeletal muscles (Figure 3; Table 3, Supplementary Table S1). Physiological changes in both the brain and heart can affect the SUVs measured from two PET scans acquired at different time points. This may include changes in blood flow, metabolism, and cardiac function [32–36], which are most likely to occur within the 90 min between the two scans. Notably, in all healthy controls, skeletal muscle uptake was somewhat higher in the test (LD) than in the retest (STD) acquisition (8%, Table 3). This decrease in muscle uptake during the retest protocol could indicate reduced stress and tension levels [37] in participants, who may have relaxed after undergoing the protocol once before. The intra-subject differences in brain, adrenal glands, and skeletal muscle SUVs for LD/STD acquisitions were found only in the healthy cohort (Figure 5; Table. 5), likely because of the increased variability provided by its larger cohort size than that of the patients (Table 1). Inaccurate segmentations may have altered some results as well. For example, adrenal gland uptakes might have been affected by segmentation errors due to their small

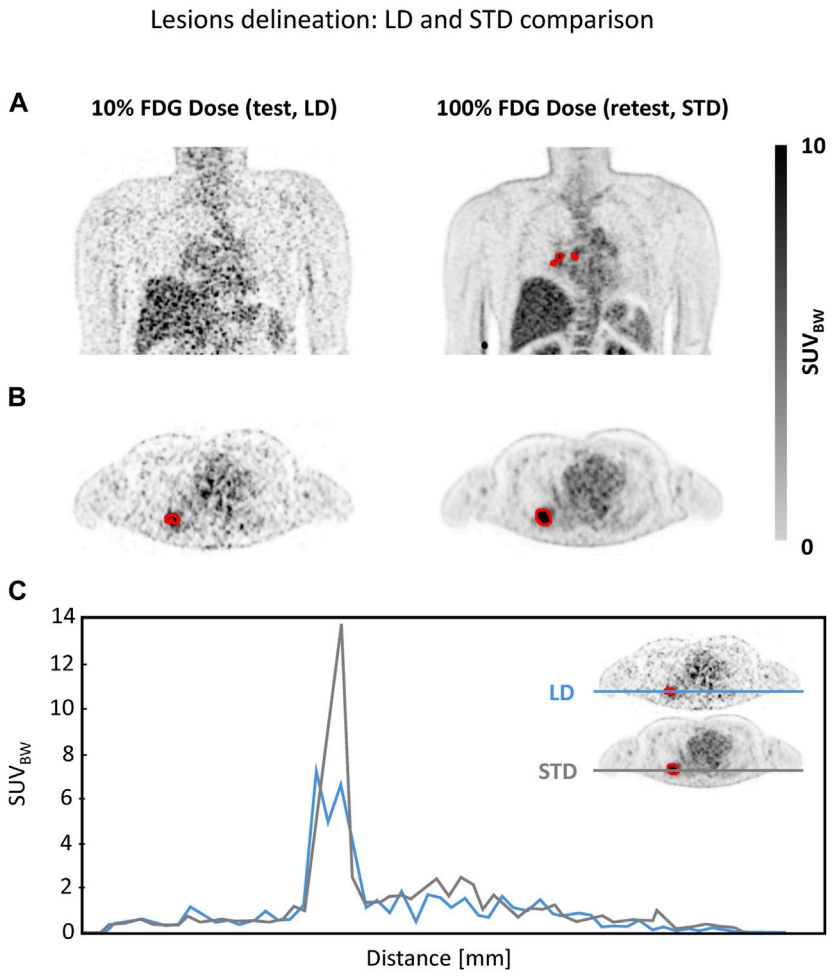

FIGURE 6
Visual comparison of lesion delineation on **(A)** coronal and **(B)** transverse images of LD and STD protocols of Pat-001. The LD images failed to detect the smallest fluoro-2-deoxy-D-glucose (FDG)-positive lesions. The primary lesion delineation in the LD image is smaller in volume and different in shape from the corresponding lesion delineation in the STD image. **(C)** Line profiles of the lesion segmented from the transverse LD (blue) and STD (gray) PET image of Pat-001.

size and low contrast with surrounding tissues, posing a challenge in distinguishing them from other structures, such as the kidneys and the liver [18], in the LD-CT image.

Imaging of lung cancer patients showed similar mean SUV_{BW} between LD and STD scans in all segmented organs. However, fewer FDG-avid lesions were identified on LD-PET images than on STD-PET images (Figure 6). Given the increased image noise levels in LD imaging, only 10 lesions were delineated from the LD images (at 10% activity injection), while 17 lesions were subsequently identified on the STD acquisitions. Specifically, delineations of seven smaller lesions (<2 cm^3) were not possible from LD images, given the increased noise level (Figure 6). In addition, the volumes of lesions were generally smaller in segmentations obtained from LD images due to reduced image quality. Nonetheless, the SUV_{BW} values of the corresponding lesions were similar in the LD and STD acquisitions, with a mean % difference equal to 10% (Table 6).

Overall, these findings suggest that low-dose FDG-PET/CT imaging may be a valuable option for reducing radiation exposure in FDG-PET/CT imaging for composing a normative database of healthy control values [9]. Our SUV_{BW} readouts for both STD and LD acquisitions were similar to published literature values [22–24]. Although variations in the mean SUV_{BW} values in organs with high metabolic activity and glucose turnover, such as the brain and the heart, were observed, the results were still consistent with the references in terms of both mean values and the minimum and maximum ranges of SUV_{BW} reported (Figure 7).

Effective doses from STD-PET were also consistent with established references for the standard clinical practice [28, 29]. Administering an activity that is 90% lower than that of the standard dose resulted in a 67% reduction in the total effective dose in healthy controls, thus effectively addressing concerns regarding radiation exposure in FDG-PET/CT imaging, particularly for non-clinical indications.

Exposure from CT plays a significant role in the overall effective dose during a standard examination. Using contrast-enhanced dual-phase CT (STD-CT) in cancer patients contributed 79% to their total effective dose, which, instead, was drastically reduced with the low-dose CT (2 mSv) protocol (Table 7). Mostafapour et al. demonstrated that the radiation dose in CT imaging could be further reduced from an effective dose of 2.6 mSv to less than 0.1 mSv by incorporating a tin filter for noise reduction [31].

10.3389/fphy.2024.1378521

TABLE 6 Mean SUV_{BW} statistics of delineated lesions. Average value and P value are indicated in bold.

Lesion ID	Test LD SUV_{BW}	Retest STD SUV_{BW}	Absolute difference
Pat-001_vol1	9.1 ± 1.6	5.9 ± 2.8	42%
Pat-001_vol2	-	6.0 ± 1.7	-
Pat-001_vol3	-	5.8 ± 1.4	-
Pat-001_vol4	-	3.6 ± 1.0	-
Pat-001_vol5	-	4.9 ± 0.6	-
Pat-002_vol1	2.6 ± 0.3	2.4 ± 0.4	9%
Pat-003_vol1	5.9 ± 0.6	6.4 ± 1.0	8%
Pat-003_vol2	-	2.6 ± 0.2	-
Pat-003_vol3	-	4.1 ± 1.0	-
Pat-003_vol4	-	3.1 ± 0.6	-
Pat-004_vol1	8.6 ± 2.6	8.5 ± 2.7	1%
Pat-006_vol1	8.0 ± 2.1	7.5 ± 2.3	7%
Pat-006_vol2	8.2 ± 2.3	7.5 ± 2.2	9%
Pat-006_vol3	7.1 ± 1.2	6.4 ± 1.4	10%
Pat-006_vol4	10.0 ± 2.8	8.0 ± 3.0	22%
Pat-006_vol5	6.5 ± 0.8	6.6 ± 1.4	1%
Pat-007_vol1	5.1 ± 0.6	4.9 ± 0.5	5%
Average			**(10 ± 14) %**
Paired T-test			**p = 0.49**

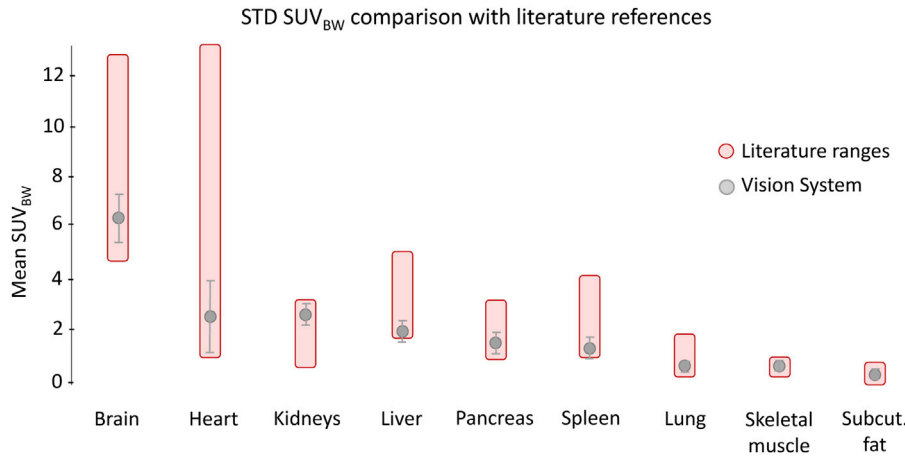

FIGURE 7
Mean SUV_{BW} comparison from STD acquisitions of healthy controls (Siemens Biograph Vision 600; gray). Red bars represent the literature ranges of minimum and maximum SUV_{BW} from [22–24].

However, potential artifacts from noise amplification during CT-based attenuation and scatter correction await further study.

Our study has several limitations. First, it was constrained by its small sample size. A larger cohort of participants could yield more reliable statistical results. Lesion delineation was performed by a single clinician, thus introducing a subjective bias into volume segmentations. The use of average delineations by multiple clinicians would offer a more precise reference. Next, LD PET imaging resulted in lower image quality, compromising its validity for clinical indications. Our study did not explore techniques to reduce noise in LD-PET images, such as AI-based image denoising methods [38, 39] or adjusted image reconstruction parameters for enhanced diagnostic accuracy [12, 40]. In our study, the

TABLE 7 Dose reports of participants in LD and STD acquisitions.

Test (LD acquisition)	ED_{CT} [mSv]	ED_{PET} [mSv]	ED_{TOT} [mSv]
Controls	2.0 ± 0.3	0.5 ± 0.1	2.5 ± 0.3
Patients	1.9 ± 0.2	0.5 ± 0.1	2.4 ± 0.1
Retest (STD acquisition)			
Controls	2.0 ± 0.3	4.8 ± 0.3	6.7 ± 0.4
Patients	16.6 ± 5.4	4.6 ± 0.3	21.3 ± 5.4

retest protocol started 90 min after the test injection, followed by an additional hour of dynamic acquisition before static reconstruction. During this period, a portion of LD activity remains undecayed and may exert a minor influence on the subsequent quantification of STD uptakes. Considering our initial injected LD activity of 28 MBq and the behavior of [18F]FDG kinetic signals at long uptake times [41–43], we anticipate an impact smaller than 5% at the time of STD static acquisition on our uptake quantifications. Last, the present study focused solely on the analysis of static images, neglecting the dynamic information of PET images. For instance, Liu et al. demonstrated that whole-body dynamic PET imaging with a 10-fold reduction in injected activity could provide relevant kinetic metrics of [18F]FDG and comparable image contrast to full-activity imaging [44]. The parametric assessment of LD-PET could contribute valuable information to the evaluation of a reference database of normal PET values in healthy controls.

Conclusion

The study demonstrated that a reduction of 90% in the administered [18F]FDG activity is feasible for semi-quantitative whole-body PET/CT imaging without loss of accuracy of organ-based SUV_{BW} assessment. LD and STD injections provided comparable mean SUV_{BW} of organs in both healthy controls and lung cancer patients, except in organs with fast a [18F]FDG turnover. However, LD images did not provide sufficient clinical quality for the diagnostic assessment of lung cancer patients. Thus, our study supports the general adoption of LD-PET/CT imaging data for imaging healthy controls for the purpose of building an organ-based normative database.

Data availability statement

The original contributions presented in the study are included in the article/Supplementary Material; further inquiries can be directed to the corresponding author.

Ethics statement

The studies involving humans were approved by the Ethics Committee of the Medical University of Vienna (EK1907/2020). The studies were conducted in accordance with the local legislation and institutional requirements. The participants provided their written informed consent to participate in this study.

Author contributions

DF: writing–original draft and writing–review and editing. LS: writing–original draft and writing–review and editing. ZC: writing–original draft and writing–review and editing. BG: writing–original draft and writing–review and editing. DG: writing–original draft and writing–review and editing. SG: writing–original draft and writing–review and editing. MH: writing–original draft and writing–review and editing. HK: writing–original draft and writing–review and editing. KK: writing–original draft and writing–review and editing. MI: writing–original draft and writing–review and editing. WL: writing–original draft and writing–review and editing. JY: writing–original draft and writing–review and editing. IR: writing–original draft and writing–review and editing. TB: writing–original draft and writing–review and editing.

Funding

The author(s) declare that financial support was received for the research, authorship, and/or publication of this article. DF and JY were supported through research funding from the Austrian Science Fund (FWF): I 5902-B. This research was funded in whole or in part by the Austrian Science Fund (FWF) [10.55776/I5902]. SG is supported by a joint research agreement between Siemens Healthineers and the Medical University Vienna. The funder Siemens Healthineers was not involved in the study design, analysis, interpretation of data, the writing of this article or the decision to submit it for publication. For open-access purposes, the authors have applied a CC BY public copyright license to any author-accepted manuscript version arising from this submission.

Acknowledgments

The authors thank Harald Ibeschitz, Ingrid Leitinger, and Rainer Bartosch for their contributions to this project. In addition to acquiring the PET/CT images of the participants, they provided valuable input and assistance in the development of this study.

Conflict of interest

The authors declare that the research was conducted in the absence of any commercial or financial relationships that could be construed as a potential conflict of interest.

The author(s) declared that they were an editorial board member of Frontiers, at the time of submission. This had no impact on the peer review process and the final decision.

Publisher's note

All claims expressed in this article are solely those of the authors and do not necessarily represent those of their affiliated organizations, or those of the publisher, the editors, and the reviewers. Any product that may be evaluated in this article, or claim that may be made by its manufacturer, is not guaranteed or endorsed by the publisher.

Supplementary material

The Supplementary Material for this article can be found online at: https://www.frontiersin.org/articles/10.3389/fphy.2024.1378521/full#supplementary-material

References

1. Beyer T, Townsend DW, Brun T, Kinahan PE, Charron M, Roddy R, et al. A combined PET/CT scanner for clinical oncology. *J Nucl Med* (2000) 41:1369–79.

2. Bastiaannet E, Groen H, Jager PL, Cobben DCP, van der Graaf WTA, Vaalburg W, et al. The value of FDG-PET in the detection, grading and response to therapy of soft tissue and bone sarcomas; a systematic review and meta-analysis. *Cancer Treat Rev* (2004) 30:83–101. doi:10.1016/j.ctrv.2003.07.004

3. Townsend DW. Dual-modality imaging: combining anatomy and function. *J Nucl Med* (2008) 49:938–55. doi:10.2967/jnumed.108.051276

4. Wechalekar K, Sharma B, Cook G. PET/CT in oncology—a major advance. *Clin Radiol* (2005) 60:1143–55. doi:10.1016/j.crad.2005.05.018

5. Spencer BA, Berg E, Schmall JP, Omidvari N, Leung EK, Abdelhafez YG, et al. Performance evaluation of the uEXPLORER total-body PET/CT scanner based on NEMA NU 2-2018 with additional tests to characterize PET scanners with a long axial field of view. *J Nucl Med* (2021) 62:861–70. doi:10.2967/jnumed.120.250597

6. Nadig V, Herrmann K, Mottaghy FM, Schulz V. Hybrid total-body pet scanners—current status and future perspectives. *Eur J Nucl Med Mol Imaging* (2022) 49:445–59. doi:10.1007/s00259-021-05536-4

7. van Sluis J, van Snick JH, Brouwers AH, Noordzij W, Dierckx RAJO, Borra RJH, et al. EARL compliance and imaging optimisation on the Biograph Vision Quadra PET/CT using phantom and clinical data. *Eur J Nucl Med Mol Imaging* (2022) 49:4652–60. doi:10.1007/s00259-022-05919-1

8. Sundar LKS, Hacker M, Beyer T. Whole-body PET imaging: a catalyst for whole-person research? *J Nucl Med* (2022) 64:197–9. doi:10.2967/jnumed.122.264555

9. Gutschmayer S, Muzik O, Hacker M, Ferrara D, Zuehlsdorff S, Newiger H, et al. Towards holistic assessment of human physiology: fully-automated construction of tracer independent total-body PET/CT normative database using diffeomorphisms [abstract]. In: Annual Congress of the European Association of Nuclear Medicine; October 15-19; Barcelona, Spain. Springer Science and Business Media LLC (2022). 225–6.

10. Tan H, Cai D, Sui X, Qi C, Mao W, Zhang Y, et al. Investigating ultra-low-dose total-body [18F]-FDG PET/CT in colorectal cancer: initial experience. *Eur J Nucl Med Mol Imaging* (2022) 49:1002–11. doi:10.1007/s00259-021-05537-3

11. Calderón E, Schmidt FP, Lan W, Castaneda-Vega S, Brendlin AS, Trautwein NF, et al. Image quality and quantitative PET parameters of low-dose [18F]FDG PET in a long axial field-of-view PET/CT scanner. *Diagnostics (Basel)* (2023) 13:3240. doi:10.3390/diagnostics13203240

12. Kertész H, Beyer T, London K, Saleh H, Chung D, Rausch I, et al. Reducing radiation exposure to paediatric patients undergoing [18F]FDG-PET/CT imaging. *Mol Imaging Biol* (2021) 23:775–86. doi:10.1007/s11307-021-01601-4

13. Prieto E, García-Velloso MJ, Rodríguez-Fraile M, Morán V, García-García B, Guillén F, et al. Significant dose reduction is feasible in FDG PET/CT protocols without compromising diagnostic quality. *Phys Med* (2018) 46:134–9. doi:10.1016/j.ejmp.2018.01.021

14. Tan H, Qi C, Cao Y, Cai D, Mao W, Yu H, et al. Ultralow-dose [18F]FDG PET/CT imaging: demonstration of feasibility in dynamic and static images. *Eur Radiol* (2023) 33:5017–27. doi:10.1007/s00330-023-09389-3

15. Kinahan PE, Fletcher JW. Positron emission tomography-computed tomography standardized uptake values in clinical practice and assessing response to therapy. *Semin Ultrasound CT MR* (2010) 31:496–505. doi:10.1053/j.sult.2010.10.001

16. van Sluis J, de Jong J, Schaar J, Noordzij W, van Snick P, Dierckx R, et al. Performance characteristics of the digital Biograph vision PET/CT system. *J Nucl Med* (2019) 60:1031–6. doi:10.2967/jnumed.118.215418

17. Wachabauer D, Beyer T, Ditto M, Gallowitsch H-J, Hinterreiter M, Ibi B, et al. Diagnostic Reference Levels for nuclear medicine imaging in Austria: a nationwide survey of used dose levels for adult patients. *Z Med Phys* (2022) 32:283–95. doi:10.1016/j.zemedi.2021.11.007

18. Sundar LKS, Yu J, Muzik O, Kulterer OC, Fueger B, Kifjak D, et al. Fully automated, semantic segmentation of whole-body 18F-FDG PET/CT images based on data-centric artificial intelligence. *J Nucl Med* (2022) 63:1941–8. doi:10.2967/jnumed.122.264063

19. Boellaard R, O'Doherty MJ, Weber WA, Mottaghy FM, Lonsdale MN, Stroobants SG, et al. FDG PET and PET/CT: EANM procedure guidelines for tumour PET imaging: version 1.0. *Eur J Nucl Med Mol Imaging* (2010) 37:181–200. doi:10.1007/s00259-009-1297-4

20. Fedorov A, Beichel R, Kalpathy-Cramer J, Finet J, Fillion-Robin J-C, Pujol S, et al. 3D slicer as an image computing platform for the quantitative imaging network. *Magn Reson Imaging* (2012) 30:1323–41. doi:10.1016/j.mri.2012.05.001

21. Otsu N. A threshold selection method from gray-level histograms. *IEEE Trans Syst Man Cybern* (1979) 9:62–6. doi:10.1109/tsmc.1979.4310076

22. Zincirkeser S, Sahin E, Halac M, Sager S. Standardized uptake values of normal organs on 18F-fluorodeoxyglucose positron emission tomography and computed tomography imaging. *J Int Med Res* (2007) 35:231–6. doi:10.1177/147323000703500207

23. Dias AH, Hansen AK, Munk OL, Gormsen LC. Normal values for 18F-FDG uptake in organs and tissues measured by dynamic whole body multiparametric FDG PET in 126 patients. *EJNMMI Res* (2022) 12:15. doi:10.1186/s13550-022-00884-0

24. Oliveira AL, Azevedo DC, Bredella MA, Stanley TL, Torriani M. Visceral and subcutaneous adipose tissue FDG uptake by PET/CT in metabolically healthy obese subjects. *Obesity (Silver Spring)* (2015) 23:286–9. doi:10.1002/oby.20957

25. Martí-Climent JM, Prieto E, Morán V, Sancho L, Rodríguez-Fraile M, Arbizu J, et al. Effective dose estimation for oncological and neurological PET/CT procedures. *EJNMMI Res* (2017) 7:37. doi:10.1186/s13550-017-0272-5

26. Huda W, Magill D, He W. CT effective dose per dose length product using ICRP 103 weighting factors. *Med Phys* (2011) 38:1261–5. doi:10.1118/1.3544350

27. Mattsson S, Johansson L, Leide Svegborn S, Liniecki J, Noßke D, Stabin M, et al. Radiation dose to patients from radiopharmaceuticals (2024). Available at: https://www.icrp.org/docs/Radiation%20Dose%20to%20Patients%20from%20Radiopharmaceuticals%20-%20A%20fourth%20addendum%20to%20ICRP%20Publication%2053.pdf (Accessed March 25, 2024).

28. Brix G, Lechel U, Glatting G, Ziegler SI, Münzing W, Müller SP, et al. Radiation exposure of patients undergoing whole-body dual-modality 18F-FDG PET/CT examinations. *J Nucl Med* (2005) 46:608–13.

29. Avramova-Cholakova S, Ivanova S, Petrova E, Garcheva M, Vassileva J. Patient doses from PET-CT procedures. *Radiat Prot Dosimetry* (2015) 165:430–3. doi:10.1093/rpd/ncv128

30. Sabri ASA, Wong JHD. Estimation of effective dose for whole body 18F-FDG PET/CT examination. *J Phys Conf Ser* (2019) 1248:012006. doi:10.1088/1742-6596/1248/1/012006

31. Mostafapour S, Greuter M, van Snick JH, Brouwers AH, Dierckx RAJO, van Sluis J, et al. Ultra-low dose CT scanning for PET/CT. *Med Phys* (2024) 51:139–55. doi:10.1002/mp.16862

32. Camargo EE, Szabo Z, Links JM, Sostre S, Dannals RF, Wagner HN, Jr. The influence of biological and technical factors on the variability of global and regional brain metabolism of 2-[18F]fluoro-2-deoxy-D-glucose. *J Cereb Blood Flow Metab* (1992) 12:281–90. doi:10.1038/jcbfm.1992.38

33. Minamimoto R. Series of myocardial FDG uptake requiring considerations of myocardial abnormalities in FDG-PET/CT. *Jpn J Radiol* (2021) 39:540–57. doi:10.1007/s11604-021-01097-6

34. Schaefer SM, Abercrombie HC, Lindgren KA, Larson CL, Ward RT, Oakes TR, et al. Six-month test-retest reliability of MRI-defined PET measures of regional cerebral glucose metabolic rate in selected subcortical structures. *Hum Brain Mapp* (2000) 10:1–9. doi:10.1002/(sici)1097-0193(200005)10:1<1::aid-hbm10>3.0.co;2-o

35. Shiyam SLK, Muzik O, Rischka L, Hahn A, Lanzenberger R, Hienert M, et al. Promise of fully integrated PET/MRI: noninvasive clinical quantification of cerebral glucose metabolism. *J Nucl Med* (2020) 61:276–84. doi:10.2967/jnumed.119.229567

36. Thut DP, Ahmed R, Kane M, Djekidel M. Variability in myocardial metabolism on serial tumor (18)F-FDG PET/CT scans. *Am J Nucl Med Mol Imaging* (2014) 4:346–53.

37. Karunanithi S, Soundararajan R, Sharma P, Naswa N, Bal C, Kumar R. Spectrum of physiologic and pathologic skeletal muscle 18F-FDG uptake on PET/CT. *Am J Roentgenology* (2015) 205:W141–9. doi:10.2214/ajr.14.13457

38. Weyts K, Lasnon C, Ciappuccini R, Lequesne J, Corroyer-Dulmont A, Quak E, et al. Artificial intelligence-based PET denoising could allow a two-fold reduction in [18F]FDG PET acquisition time in digital PET/CT. *Eur J Nucl Med Mol Imaging* (2022) 49:3750–60. doi:10.1007/s00259-022-05800-1

39. Boudjelal A, Elmoataz A, Attallah B, Messali Z. A novel iterative MLEM image reconstruction algorithm based on beltrami filter: application to ECT images. *Tomography* (2021) 7:286–300. doi:10.3390/tomography7030026

40. Kertész H, Traub-Weidinger T, Cal-Gonzalez J, Rausch I, Muzik O, Shyiam Sundar LK, et al. Feasibility of dose reduction for [18F]FDG-PET/MR imaging of patients with non-lesional epilepsy. *Nuklearmedizin* (2023) 62:200–13. doi:10.1055/a-2015-7785

41. Wangerin KA, Muzi M, Peterson LM, Linden HM, Novakova A, O'Sullivan F, et al. Effect of 18F-FDG uptake time on lesion detectability in PET imaging of early stage breast cancer. *Tomography* (2015) 1:53–60. doi:10.18383/j.tom.2015.00151

42. Chin BB, Green ED, Turkington TG, Hawk TC, Coleman RE. Increasing uptake time in FDG-PET: standardized uptake values in normal tissues at 1 versus 3 h. *Mol Imaging Biol* (2009) 11:118–22. doi:10.1007/s11307-008-0177-9

43. Laffon E, Adhoute X, de Clermont H, Marthan R. Is liver SUV stable over time in 18F-FDG PET imaging? *J Nucl Med Technol* (2011) 39:258–63. doi:10.2967/jnmt.111.090027

44. Liu G, Hu P, Yu H, Tan H, Zhang Y, Yin H, et al. Ultra-low-activity total-body dynamic PET imaging allows equal performance to full-activity PET imaging for investigating kinetic metrics of 18F-FDG in healthy volunteers. *Eur J Nucl Med Mol Imaging* (2021) 48:2373–83. doi:10.1007/s00259-020-05173-3